Poly(glycidyl methacrylate) macromolecular assemblies as biocompatible nanocarrier for the antimicrobial lysozyme

Poly(glycidyl methacrylate) macromolecular assemblies as biocompatible nanocarrier for the antimicrobial lysozyme

Miguel Palenzuela[1], Laura Valenzuela[2], Georgiana Amariei[2,*], Juan F. Vega[3], Marta E.G. Mosquera[1,*], Roberto Rosal[2]

[1] Department of Organic and Inorganic Chemistry, Institute of Chemical Research "Andrés M. del Río" (IQAR), Universidad de Alcalá, 28805 Alcalá de Henares, Madrid, Spain
[2] Department of Chemical Engineering, Universidad de Alcalá, 28805 Alcalá de Henares, Madrid, Spain.
[3] Department of Macromolecular Physics, Instituto de Estructura de la Materia, IEM-CSIC, 28006 Madrid, Spain

[*] Corresponding Authors georgiana.amairie@uah.es, martaeg.mosquera@uah.es

Keywords: *Poly(glycidyl methacrylate); Macromolecular assembly; Nanocarrier; Lysozyme; Antibacterial surface, Biocompatible coating*

Abstract

The antimicrobial lysozyme (Lys) was electrostatically incorporated to negatively charged crosslinked poly(glycidyl methacrylate) (c-PGMA) macromolecular assemblies. The resulting material was characterized by AFM, infrared spectra, water contact angle measurements and the staining with the primary amino specific dye fluorescamine. c-PGMA nanoparticles were successfully loaded with Lys reaching ratios of 27.3 ± 4.0 and 22.5 ± 1.7 mg Lys/g polymer for c-PGMA suspensions and functionalized glass substrates, respectively. Lys-loaded c-PGMA caused clear inhibition zones on *S. aureus* and *E. coli* in comparison to neat c-PGMA. c-PGMA functionalized surfaces were intrinsically resistant to colonization, but the incorporation of Lys added resistance to bacterial attachment and allowed keeping surfaces clean of bacterial cells for both strains. A relatively rapid release (24 h) of Lys was observed at physiological pH (7.4). In addition, c-PGMA functionalized substrates could be reloaded several times without losing capacity. c-PGMA macromolecular assemblies did not display cytotoxicity to human dermal fibroblasts as shown in 24 h MTT assays. This work demonstrated that c-PGMA assemblies display durable antibacterial activity, biocompatibility, and full reloading capacity with antimicrobial peptides. c-PGMA functionalized materials have potential application as nanocarriers for anti-infective uses.

1. Introduction

The emergence of pathogens resistant to the existing drugs is a hot topic in science and a major threat to healthcare systems. A recent study estimated that >33,000 deaths might be directly attributed to infections with antibiotic-resistant bacteria every year only in the EU (Cassini et al., 2019). Emerging pathogens, and antimicrobial resistances are not new because bacteria have the evolutive capacity to acquire mechanisms to confront multiple stressors. However, the scarcity of new antibiotic molecules and the abusive use of the existing ones is a major cause for concern, particularly concerning gram-negative bacteria, which are currently posing the greatest threat (Duval et al., 2019). Accordingly, the search for new antibacterial strategies and the implementation of public health policies aimed at reducing the exposure of microorganisms to antibiotics are acknowledged priorities. Pathogens not only appear in planktonic form. In fact, they are more dangerous when colonizing surfaces by forming biofilms. Biofilms are complex microbial communities that grow adhered to a substrate embedded in a matrix of extracellular polymeric substance (Flemming and Wingender, 2010). Biofilms display a complex three-dimensional organization very different from individual planktonic cells, which is very efficient to protect bacteria from environmental stressors (de la Fuente-Núñez et al., 2013). Once formed, biofilms are very difficult to eradicate with the usual antimicrobial agents. This fact explains the efforts paid to the design of surfaces that avoid or make difficult the initial attachment of biofilm-forming microorganisms.

The development of nanotechnology offers a new paradigm to fight against pathogens. Different nanoparticles (NP) have been proposed as antimicrobials alternative or combined to traditional substances (Liu et al., 2019). NPs benefit from high surface-to-volume ratio, high reactivity and the possibility to cross cell membranes to impair bacteria using different mechanisms, which include oxidative stress induction, metal ion release, ribosome destabilization, and interference with DNA replication, among others (Ogunsona et al., 2020; Wang et al., 2017). Besides, NPs can promote the action of antibiotics by enhancing membrane permeability,

thereby allowing the use of lower antibiotic doses (Vázquez-Muñoz et al., 2019). NPs have also been proposed as efficient drug carriers to reduce the degradation of pharmaceuticals under physiological conditions, to decrease in vivo toxicity profiles, and to increase their bioavailability at the target site (Wilczewska et al., 2012). NP-based antimicrobial delivery systems transfer high doses of drugs to the site of infection or keep a continuous release profile for extended periods, which are strategies to overcome antimicrobial resistance. Many nanomaterials, including mesoporous silica, carbon-based materials, liposomes, solid-lipid NPs, dendrimers and other polymeric NPs have been proposed for this task (Deng et al., 2020)

Polymer-based NPs have attracted attention because of their easy functionalization and stability in biological environments (Gumustas et al., 2017). Advanced polymeric materials can be engineered in many different ways for applications in personalized and precision therapies (Mitchell et al., 2020). Polymer-based nanocarriers for antimicrobial agents can be polymeric micelles, dendrimers, nanocapsules, and nanospheres (Sur et al., 2019). According to their loading nature nanocarriers can be classified into surface loading, matrix loading, pore loading and conjugates or molecular-level docking systems. In most cases, the drug is loaded through non-covalent interactions such as electrostatic self-assembly, van der Waals forces, or hydrogen bonding, for easier delivery. Besides, certain intermediates like surfactants or other capping agents may be used to enhance the compatibility between polymeric surface and drug (Wang et al., 2019). Abdelghany et al. (2012) prepared poly(lactide-co-glycolide) (PLGA) loaded with the aminoglycoside antibiotic gentamicin. The loading of gentamicin into the hydrophobic PLGA matrix was improved at high pH values, at which the amino moieties of the antibiotic were deprotonated (Abdelghany et al., 2012). In another study, the emulsification solvent diffusion method was used to encapsulate an antimicrobial into PLGA NPs for the eradication of biofilms of *Staphylococcus aureus* and *Pseudomonas aeruginosa* (de Mélo-Silva et al., 2020). The antimalarial halofantrine was loaded into poly(ethylene glycol) surface-modified polylactide nanocapsules, allowing a sustained release and a better control of parasite *Plasmodium berghei* (Mosqueira et al., 2004).

Antimicrobial peptides and proteins (AMP) constitute a family of molecules that create a natural protection against pathogenic organisms (Zhang and Gallo, 2016). The antibacterial capacity of AMPs is generally associated to their positive charge, which favours the interaction with the negatively charged bacterial membranes. In most cases, AMP cause membrane disruption and their activity towards different species is due to different structure of the outer envelopes of different microbes, although certain AMP can cross the bacterial membranes and impair enzyme activity or other intracellular functions (Le et al., 2017). Lysozyme is a glycoside hydrolase that catalyses the hydrolysis of 1,4-beta-linkages of peptidoglycan. Peptidoglycan is the main component of the outer the cell wall of gram-positive bacteria and consists of glycan chains of N-acetylglucosamine and N-acetylmuramic acids crosslinked with peptide side chains. Gram-negative bacteria possess a thinner peptidoglycan layer but surrounded by an outer envelope consisting mainly of lipopolysaccharides (Silhavy et al., 2010). The hydrolysis of peptidoglycan causes the disruption of cell walls eventually leading to the cell lysis. Besides, its enzymatic activity, lysozyme is cationic and interacts with the negatively charged moieties of bacterial outer walls. Gram-positive bacteria are negatively charged due to the presence of teichoic acids linked to peptidoglycans, while the negative charge of lipopolysaccharides confers an overall negative charge to gram-negative bacteria (Ragland and Criss, 2017). The use of AMP for functionalizing different materials has been proposed elsewhere. Lysozyme, in particular has been immobilized onto electrospun nanofibrous scaffolds to create wound dressings with antibacterial activity sustained for at least 14 days (Amariei et al., 2018). Surfaces functionalized with biotinylated lysozyme previously coated with streptavidin receptors proved high antibacterial efficiency against Micrococcus luteus (Beaussart et al., 2021).

In this work, we used a novel polymeric macromolecular assembly of NPs prepared by covalent crosslinking of the network of combs obtained from the ring opening polymerization of glycidyl methacrylate (GMA). The obtained polymer consist of flexible NPs of crosslinked poly(glycidyl methacrylate), c-PGMA. The material was used to functionalize a surface that acted as carrier for the AMP lysozyme. This assembly of NPs provided a rechargeable antimicrobial coating that also showed resistance to bacterial colonization as demonstrated using strains of *Escherichia coli* and *Staphylococcus aureus*. The such developed lysozyme-loaded-cPGMA functional material ca be used in a wide range of biomedical applications such as (i) drug/peptide delivery systems for therapeutic purposes; (ii) wound dressings; (iii) bioactive scaffolds- coatings for tissue engineering scaffolds; and (iv) bacterial responsive coatings for biomedical device- associated infections.

2. Materials and methods

2.1 Chemicals

Lysozyme (Lys, from chicken egg white, 14.4 kDa) was purchased from Sigma-Aldrich. Glycidyl methacrylate (GMA), fluorescamine, dimethyl sulfoxide (DMSO), Tween 80, polyvinylpyrrolidone (PVP), acetone, toluene, and ethanol were also obtained from Sigma-Aldrich. 3-(4,5-Dimethyl-2-thiazolyl)-2,5-diphenyl-2H-tetrazolium bromide (MTT) was procured

from Thermo Fischer Scientific. The regents of biological medium and buffers were acquired from Condalab (Madrid). Ultrapure water (Millipore Milli-Q System, >18 MW cm) was used in all experiments. GMA was dried over CaH_2 overnight, distilled under reduced pressure and stored in a flask with PTFE-valve inside a glovebox at -20 °C. The solvents used for the synthesis of catalysts were purified in a MBraun Solvent Purification System and stored over molecular sieves (4 Å) in PTFE flasks. The toluene used in polymerization reactions was also dried by refluxing over sodium for at least 48 h. No further purification was used for all the other reagents. Benzyl potassium, $[AlMe_2\{2,6\text{-}(CHPh_2)2\text{-}4\text{-}tBu\text{-}C_6H_2O\}]_n$, 2,6-bis(diphenylmethyl)-4-*tert*butylphenol, and $K\{2,6\text{-}(CHPh_2)2\text{-}4\text{-}tBu\text{-}C_6H_2O\}]$ were prepared as reported elsewhere (Lochmann et al., 1966; Muñoz et al., 2018; Searles et al., 2013)

2.2. Combined polymerization procedure of GMA

Inside a glovebox, GMA (0.38 mL, 2.79 mmol) was incorporated to a solution of $[AlMe_2\{2,6\text{-}(CHPh_2)2\text{–}4\text{-}tBu\text{-}C_6H_2O\}]$, (15 mg, 27.9 μmol) in 1.9 mL of dry toluene, and mixed under stirring for 30 min at room temperature. Then, $[KAlMe_3\{2,6\text{-}(CHPh_2)2\text{–}4\text{-}tBu\text{-}C_6H_2O\}]$, (16 mg, 27.9 μmol) was added to the mixture and stirred at 100 °C for 1 h. The polymerization was quenched with wet dichloromethane and dried in a vacuum oven at 60 °C overnight to obtain the polymer c-PGMA as a transparent solid. 1H NMR spectroscopy allowed us to confirm that total conversion of the monomer is achieved. The characterization of the final crosslinked polymer c-PGMA was carried out using IR and NMR spectroscopies, as well as DSC (see SI for details).

2.3. Nanocarrier loading and surface functionalization

The AMP Lys was incorporated to c-PGMA by electrostatic self-assembly following two different procedures: (i) for preparing polymeric dispersions, and (ii) for fabricating polymeric coatings. In order to create a homogeneous dispersion, Tween 80 and PVP were used as surfactants. Briefly, 20 mg of c-PGMA were dispersed in 500 μL acetone and, subsequently, in 10 mL of a phosphate buffer solution (0.1 M, pH 7) containing either no dispersant or 3.5 mg L-1 of surfactant followed by sonication for 10 min. The immobilization of Lys was conducted at room temperature in a stirred vessel (150 rpm) by adding 20 or 40 mg Lys to the dispersion (peptide-to-polymer weight ratio of 1 and 2, respectively). The process was carried out overnight after which the polymer was recovered by filtration. The extent of Lys charged on polymer was determined by HPLC as detailed below. The polymeric coatings were prepared by drop casting. To this end, 200 μL of a 100 mg mL^{-1} c-PGMA in acetone suspension were dropped onto 13 mm diameter pre-washed glass coverslips. After deposition, the glass substrates were dried at room temperature to evaporate the solvent, which resulted in a uniform coating. The loading with Lys was carried out at room temperature by immersing the specimens in 2 mL phosphate buffer solution containing 20 mg Lys. As for polymeric dispersions, the process took place overnight under gentle stirring. After loading, the glass coverslips were removed, rinsed with water, and desiccated at 25 °C.

2.4. Characterization techniques

Both the catalysts and the c-PGMA material were characterized by Nuclear Magnetic Resonance (NMR, Bruker 400 Ultrashield-^{1}H400 MHz, ^{13}C 101 MHz) and Fourier Transform Infrared (FTIR, Agilent Cary 630 Spectrometer) spectroscopy, at room temperature. For NMR analysis, all chemical shifts were determined using solvents residual peaks and were referenced related to TMS. FTIR spectra were collected in the 4000–650 cm^{-1} range. The morphology of the materials before and after functionalization was assessed by a scanning electron microscope (SEM, DSM950 Zeiss, Oberkochen, Germany) working at 15 kV. Prior to the observation, the sample surfaces were coated with gold. Surface hydrophilicity was determined by means of Water Contact Angles (WCA, Krüss DSA25 Drop Shape Analysis System), measured at room temperature. The amount of Lys loaded per unit mass of polymer was determined by HPLC using an Agilent LC 1260 system with diode array detection, as detailed below. First, the Lys loaded specimens were incubated for 24 h in acidic water (pH 2) ensuring the total detachment of peptide from the surface (Kaisersberger-Vincek et al., 2016). The analysis of Lys was performed at room temperature using a Protein Green C4 (5 μm, 150 × 4.6 mm) at a flow rate of 1 mL min^{-1} with a linear gradient of acetonitrile-Milli-Q water (with TFA acid, 0.1% v/v) ranging from 20% to 80%.

Fluorescamine staining of primary amino groups was used to assess the presence of Lys on functionalized surfaces. For it, glass discs were incubated for 15 min at ambient temperature with 50 μL of fluorescamine solution (100 mg mL^{-1} in ethanol) in the dark. The fluorescamine labelled molecules were visualized using confocal laser scanning microscopy (CLSM) in a Carl Zeiss LSM5100 instrument, at excitation and emission wavelengths of 365 nm and 470 nm respectively.

Differential Scanning Calorimetry. DSC measurements were performed on a Mettler Toledo DSC 3 apparatus. Samples were placed into aluminium crucibles and measured at temperatures ranging from -20 to 100 °C at heating and cooling rates of 10 °C/min. Particle size and ζ-potential of c-PGMA suspension in ultrapure water (pH 7.0 ± 0.1) were determined by dynamic light scattering (DLS) and electrophoretic light scattering with a Zetasizer Nano ZS (Malvern Instruments, Worcestershire, UK) at 25 °C.

Atomic force microscopy (AFM) imaging of the films prepared in Section 2.3 was carried out using a μTA™ 2990 Micro-Thermal Analyser (TA Instruments, Inc.,

New Castle, DE, USA). Topography micrographs were recorded in contact mode at room temperature. For this end, a V-shaped silicon nitride probe with a cantilever length of 200 μm and a spring constant of 0.032 N m^{-1} was used. The dimension of the images was 3 μm^2. The raw topographical data were treatment with Gwyddion image software (Nečas and Klapetek, 2012). Using this software, the surface averaged heights (Sa) and their root mean squared (Sq) have been evaluated over the complete 3D surface in a set of 5 images for each of the samples under study.

2.5. Antibacterial and antibiofilm activity

The antibacterial activity of c-PGMA and Lys-loaded c-PGMA was investigated using both gram-positive and gram-negative reference strains, such as *Staphylococcus aureus* (CECT 240) and *Escherichia coli* (CECT 516). The microorganisms were grown in Nutrient Broth (NB, 10 g L^{-1} peptone, 5 g L^{-1} beef extract, 5 g L^{-1} NaCl, pH 7.0 ± 0.2) at 37 °C under continuous stirring. Two types of bioassays were performed. Radial diffusion or halo inhibition assays tests were conducted using solid agar treated with functionalized and non-functionalized glass substrates. Coated and uncoated glass surfaces were deposited onto agar plates, previously spread with 0.4 mL of bacterial cultures containing 106 cells mL-1. Agar plates were then maintained for 14 days, in darkness, at 37 °C and photographed at predetermined time of incubation to calculate the inhibition area. Two replicates of the full process were used. Besides, colonization experiments were performed by contacting c-PGMA and Lys-loaded c-PGMA coated surfaces with 6 mL of bacterial suspensions containing 106 cells mL-1 in NB on sterile 6-well polystyrene plates. The bacterial colonization and biofilms formation was allowed within 24 h of incubation, under dark and at 37 °C.

The antimicrobial effect was assessed by Scanning Electron Microscopy (SEM). For it, the specimens were well washed in phosphate buffered saline (PBS) and dried at room temperature overnight prior to sputter gold coating. The extent of surface colonization was also determined using the staining Live/Dead Baclight Bacterial Viability Kit (Fisher Scientific). The kit contains two nuclear acid stains. SYTO9 is membrane-permeable green-fluorescent and marks viable cells, and Propidium Iodide (PI) red-marks cells with the membranes impaired. The incubation took place in darkness at 25 °C for 15–30 min using 10 μL per sample in DMSO. The surface was observed using CLSM with excitation/emission at 488/500–575 nm for SYTO9, and 561/570–620 nm for PI.

2.6. In vitro Lys release and recharging capacity

The release profile from Lys-loaded c-PGMA was assessed in PBS at pH 7.4 at and 25 ± 2 °C for 14 days. The release tests were conducted in closed glass tubes containing one c-PGMA functionalized glass disc in 2.5 mL of PBS, which was kept under orbital shaking at 100 rpm. Aliquots of 100 μL were collected at predetermined time intervals (1, 3, 6 and 10 h and 1, 2, 3, 7, 10, and 14 days) to quantify Lys. The concentration of Lys was determined by HPLC, as detailed previously. After each HPLC measurement the remaining solution was returned to the reaction tubes in order to keep the volume constant. For recharging experiments each c-PGMA coated disc was re-incubated for 24 h in a Lys solution with the same concentration. The release of Lys from reloaded samples was performed during 24 h in PBS pH 7.4. All measurements were performed by duplicates.

2.7. Biocompatibility

The cytotoxic response of c-PGMA was tested with human dermal fibroblasts (hDF, ATCC) using the colorimetric MTT assay. *In vitro* studies were performed with c-PGMA coated discs (n = 4) previously cleaned with alcohol and placed into 24-well sterile plate and seeded with cell suspensions containing 3 × 105 cells per well. Control without discs were used for comparison. The inoculated wells were incubated for 24 h under standard conditions (37 °C, 5% CO2 humidified atmosphere). After exposure, the cells were removed and incubated with MTT reagent for 4 h. The generated formazan, which is equivalent to the number of viable cells, was solubilized with DMSO and measured at 570 nm with a BioTek Elisa microplates Reader. Cell viability was expressed as reduction percentage with respect to controls.

3. Results and discussion

3.1. Characterization of nanocarriers

Two metallic catalysts were used for the polymerization of the GMA in a two-step process, in a methodology adapted from the one previously published by us (Palenzuela et al., 2019). Initially, the Lewis acid catalysts [$AlMe_2${2,6-$(CHPh_2)$2–4-tBu-C_6H_2O}] was used to perform the ring opening polymerization of GMA. Selective polymerization via oxirane ring was achieved after 30 min stirring at room temperature. Then the heterometallic compound [$KAlMe_3${2,6-$(CHPh_2)$2–4-tBu-C_6H_2O}] was added and after heating to 100 °C for 1 h the polymerization of the pendant groups was achieved (Scheme 1). The heterometallic catalyst induced the crosslinking of a significant

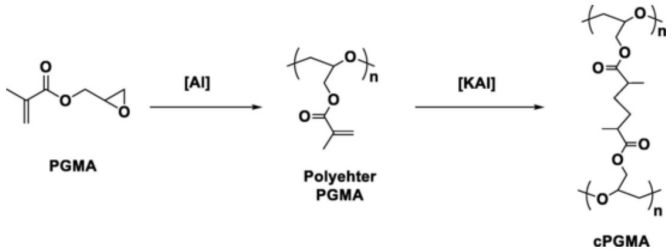

Scheme 1. Combined polymerization of glycidyl methacrylate: first, the ROP by the oxirane group with [Al] = [$AlMe_2${2,6-$(CHPh_2)$2–4-tBu-C_6H_2O}] and second, the polymerization of the pendant acrylate groups with [KAl] = [$KAlMe_3${2,6-$(CHPh_2)$2–4-tBu-C_6H_2O}].

number of the acrylate pendant groups, as shown by the band at 970 cm-1 in the IR spectra that corresponds to the wagging vibration of the acrylate double bond (Fig. 1). The new macromolecular assembly formed can be envisioned as a network of combs generated by covalent cross-linking of their backbones, further details are provided in our previously reported work (Palenzuela et al., 2019). DSC studies show a T_g value of 12 °C (See SI, Fig. S6), which indicates that the synthesized acromolecular assembly is quite flexible at room temperature. DLS measurements where performed to stablish the particle size due to the unusual morphology of these macromolecular assemblies as previously described by us (Palenzuela et al., 2019). The diameter size of the prepared c-PGMA particles was about 1550.0 ± 170.0 nm, compatible with their decoration by small molecules such as Lys (Table1).

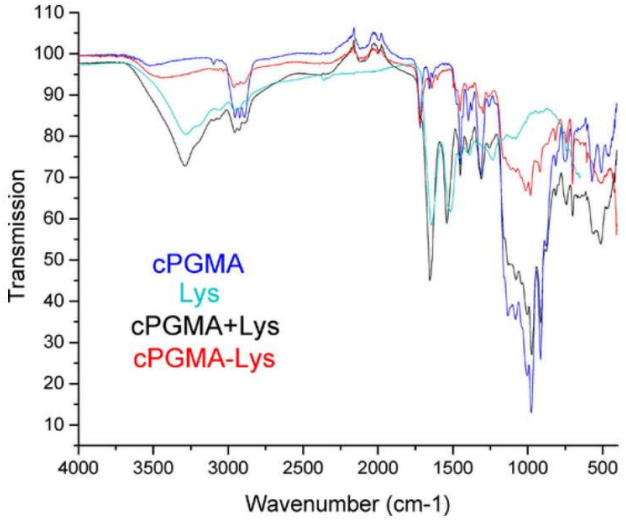

Figure 1. FTIR spectra of glass substrates loaded with (from top to bottom), Lys, c-PGMA and Lys-c-PGMA.

Table 1. Properties of c-PGMA, Lys and loaded substrates.

Particle size c-PGMA (DLS, suspension in water)	1550 ± 170 nm
Lys DLS size (pH 7)*	4.3 ± 1 nm
Zeta potential c-PGMA (pH 7)	-40 ± 5 mV
Zeta potential Lys (pH 7)**	+6.5 ± 1.0 mV
Lys-loaded c-PGMA (mass loading ratio Lys:c-PGMA, 1:1)	
Lys/c-PGMA ratio (suspension)	27.3 ± 4.0 mg/g (97.6% ± 3.4)
Lys/c-PGMA ratio (glass substrates)	22.5 ± 1.7 mg/g (95.7% ± 2.3)

* Courdouan, France. Application Note -Lysozyme- (cordouan-tech.com).
** Henry et al. (2017)

The amount of Lys loaded by c-PGMA was quantified in suspension and for c-PGMA deposited on glass substrates by HPLC as stated before. The results of Lys loading are shown in Table 1 together with other properties of the suspensions and loaded substrates. In both cases, suspension and c-PGMA immobilized on glass substrates, an increase of Lys:c-PGMA ratio in the loading suspension did not result in a proportional increase in the loaded amount. For suspensions of c-PGMA, changing the mass ratio of Lys to c-PGMA from 1:1 to 2:1 resulted in < 20% increase in the amount of Lys loaded. Similarly, for glass substrates, doubling the amount of Lys to c-PGMA increased the amount of Lys from 20.0 to 25.8 mg/g. The use of capping agents (PVP and Tween 80) only resulted in a modest <15% increase in Lys loading. Therefore, and in what follows, all described materials were loaded without any capping agents using 1:1 Lys:c-PGMA mass ratio.

The studies on the adsorption to different substrates showed that Lys tends to form a mono-layer at low surface concentration, with additional layers at higher bulk concentration (Kim and Somorjai, 2003). Depending of surface hydrophobicity and charge, the adsorption can be more or less strong. It has been shown that Lys undergoes reconfiguration but does not denature when adsorbed onto negatively charged silica. When interacting with hydrophilic surfaces, Lys does not suffer conformational changes, although its orientation may evolve from “side-on” to “end-on” configuration as concentration increases (Wertz and Santore, 2002). In the case of highly hydrophobic substrates, Lys gets more tightly bound and quickly forms a first layer of adsorbed molecules that can even lose enzymatic activity. Further layers, adsorbed with decreasing enthalpy, remain fully active (Schmidt et al., 1990). The electrostatic interaction between the negatively charged cPGMA (zeta potential -40.0 ± 5.0 mV at pH 7) and Lys (zeta potential + 6.5 ± 1.0 mV at pH 7; Henry et al., 2017) is expected to take place for pH < 11, which is the isoelectric point of Lys (Green et al., 2001). Our results demonstrated that c-PGMA functionalized surfaces reached a full surface coverage for the loading concentrations used in this work. As shown below, the relatively easy desorption of Lys from c-PGMA and the fact that it keeps its activity, indicated that the interaction of Lys with functionalized surfaces was low enough to avoid denaturation. Concerning surface hydrophobicity, the WCA of the specimens revealed a relatively hydrophobic surface, with a value of 91.8 ± 2.7 for c-PGMA on glass substrates, which dropped to 49.8 ± 2.0 upon loading with Lys (Fig. S1, Supplementary Material, SM).

The presence of Lys on the surface of c-PGMA functionalized specimens was assessed using FTIR as shown in Fig. 1. The spectrum of cPGMA shows typical bands at 1720 cm^{-1} corresponding to the carbonyl group of the ester and at 910 cm-1 for the polyether bonds, as reported previously (Palenzuela et al., 2019). The absorption at 1310 cm^{-1} can be assigned to the C O bond stretching vibration of the ester group of c-PGMA and the one at 1450 cm^{-1} corresponded to

the C C stretching vibration (Zhang et al., 2017). The FTIR spectra of Lys-loaded materials clearly showed the distinctive amide I and amide II bands characteristic of the enzyme. The amide I peak appeared near 1650 cm^{-1} and corresponds to the C O stretching of peptide linkages. The amide II peak, at about 1545 cm^{-1} is due to N H bending vibrations. The typical hydration water band of proteins appears 3300 cm^{-1} (Bridelli, 2017).

The presence of Lys onto c-PGMA functionalized surface was revealed by fluorescamine staining. The results are shown in Fig. 2 as CLSM images of specimens stained with the fluorescamine, which is a well-known method to mark the primary amines founded on the surface of proteins (Duan et al., 2017). Fluorescamine fluorescence was absent in non-Lys loaded c-PGMA but clearly observed in Lys-c-PGMA materials.

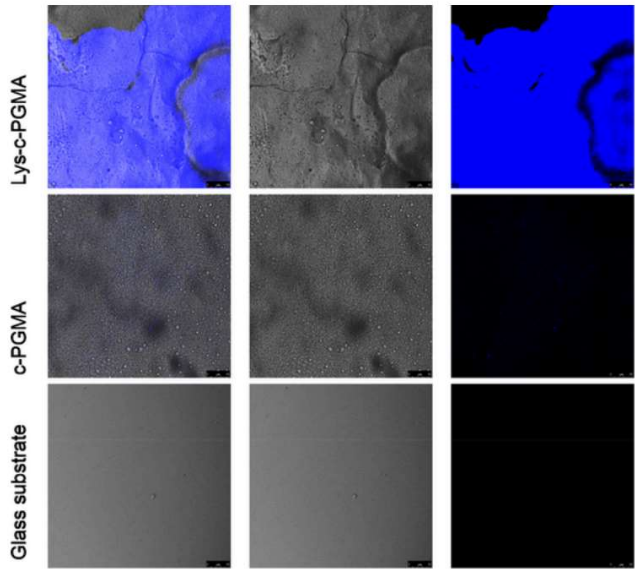

Figure 2. CLSM images of Lys-c-PGMA (after impregnation), c-PGMA (before impregnation) and bare glass substrate. Fluorescamine-conjugated Lys appears in blue. (Scale bar 50 µm).

We have analysed the protein layer formation by studying the morphological aspects of the macromolecular assemblies placed onto a glass surface using AFM in contact mode. The morphological features are revealed in the selected images of Fig. 3. Fig. 3A and B displays the 3D-topography for c-PGMA and Lys-c-PGMA samples, respectively.

The bare c-PGMA polymer surface is not flat, but it displays considerable roughness (maximum height 51 nm). It is clearly seen that the surface in c-PGMA in Fig. 3A is constituted by peaks and valleys indicating a hierarchical microstructure formed by overlapping NPs. These topographic features are consistent with closely packed "disk-shaped" NPs with a radius of around 80–100 nm and an average height of Sa = 23.3 ± 2.6 nm (Sq = 5.0 ± 0.8 nm). In Fig. 3C a profile line in a representative zone of the bare c-PGMA sample is sketched. The NPs spread onto the glass surface adopted a disk shape, indicating flexibility. The deformability is due to Tg value of 12 °C of c-PGMA.

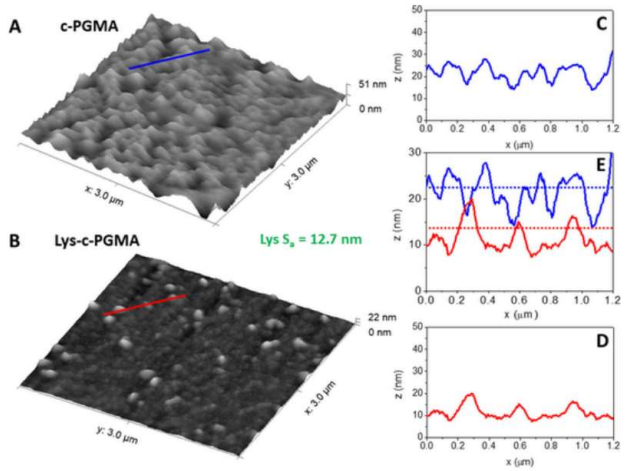

Figure 3. Surface topography images and corresponding line profiles analyses of bare c-PGMA (A, C) and Lys-c-PGMA surfaces after impregnation (B, D). (E) is the difference between the two representative profiles in C and D: the dotted lines indicate the average Sa values in c-PGMA (blue) and Lys-cPGMA (red) samples.

Representative topographical images of surface-immobilized Lys, and the corresponding profile analysis, are presented in Fig. 3B and D. The examination of AFM images of Lys-c-PGMA surface revealed that the adsorbed Lys forms a dense layer onto the polymeric surface. This makes the topographic features of the Lys-c-PGMA less prominent than those observed in the bare c-PGMA films (see Fig. 3B). The maximum height in this case is 22 nm. The evaluated surface average roughness in Fig. 3B is Sa = 10.6 ± 2.4 nm (Sq = 1.5 ± 0.4 nm), as it can be envisaged from the representative profile line of Fig. 3D. The difference measured in the average height profiles in different zones of the c-PGMA and Lys-c-PGMA samples gives rise to a thickness of around 12.7 nm of the protein layer. This result is visualized in Fig. 3E. This value suggests a considerable packing density adsorption of the protein in various layers, in agreement with the reported results on Lys adsorbed onto PBMA and glass functionalized surfaces (Dutta et al., 2011; Ivanova et al., 2006). Some authors have argued that the ability of generate this high level of adsorption in Lys and other proteins is due to the strong electrostatic interactions between the proteins and the polymeric surface if buffers with low ionic strength are used as adsorption vehicles (Buijs and Hlady, 1997).

3.2. Antimicrobial activity

The antimicrobial activity of Lys-loaded c-PGMA deposited on glass substrates was assessed by de measuring halo inhibition zone after up to 14 days in contact with cultures of *E. coli* and *S. aureus* in radial diffusion assays. A selection of representative images is included in Fig. S2 (SM), and the full quantitative results of halo zone obtained from digitally treated

photographs in shown in Fig. 4. The results showed that during the first days, the halo of inhibition was higher for *E. coli*, whereas the images taken after >10 and days of incubation showed larger inhibition area for *S. aureus*. In halo inhibition experiments, the impairment of bacterial growth is mainly governed by the diffusion of the antimicrobial compound from a reservoir. For increasing release time, the dispersion into a larger area may result in lower concentration of active compound. Therefore, longer incubation time results in higher surface exposed but at lower concentration. The results are consistent with the higher susceptibility of gram-positive rather than gram-negative bacteria when exposed to Lys. This is due to the different structure of their cell walls because Lys targets the 1,4-beta-linkages between N-acetyl-muramic acid and N-acetyl-d-glucosamine from peptidoglycan and gram-negative bacteria have their peptidoglycan protected by an outer lipopolysaccharide membrane that makes them less susceptible to Lys. Literature data are generally consistent in finding inhibition concentration values about 10 μg mL^{-1} for *S. aureus* and 1 mg mL^{-1} for *E. coli*, in line with the preceding explanation (Chen et al., 2005; Lee et al., 2013; Vahdati and Tohidi Moghadam, 2020; Ye et al., 2019).

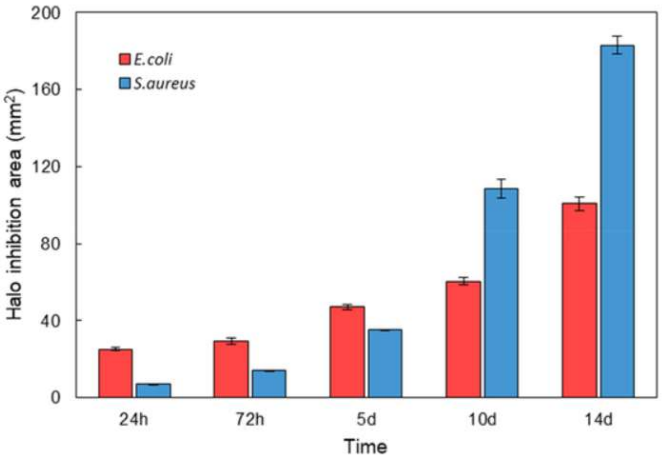

Figure 4. Halo inhibition surface for specimens in agar plates inoculated with 0.4 mL bacterial cultures containing 10^6 cells mL^{-1} of *E. coli* and *S. aureus* plates. (Temperature 37 °C.)

SEM images of cultures of both strains after 24 h at 37 °C in contact with growing bacterial cultures are shown in Fig. 5. Bare glass substrate is also included for comparison. The images showed that c-PGMA surface was much less colonized than glass. Some cells appear attached to the surface indicating difficulty for bacterial colonization that could be attributed to the hydrophobicity and negative charge of c-PGMA as indicated in Table 1. In Lys-loaded c-PGMA surface, however, the surface appears essentially free of cells, and most of the existing present shape alterations suggesting loss of cell integrity. Membrane damage was confirmed using Live-Dead staining. The images, shown in Fig. S3 (SM), indicated green-marked viable cells scattered on the surface of cPGMA, that run red-marked, membrane-damaged bacteria, in Lysloaded c-PGMA.

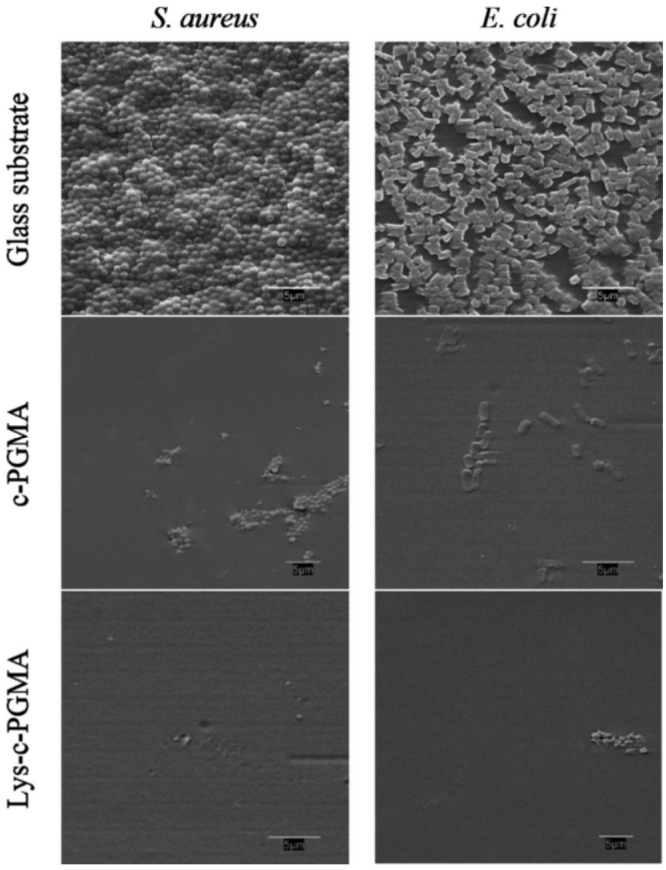

Figure 5. SEM micrographs (scale bar 5 μm) of *E. coli* and *S. aureus* biofilm for cover glass surface (control) and the cover glass with c-PGMA and Lys-loaded cPGMA after biofilm growth for 24 h

The possible cytotoxicity of the polymeric nanomaterial c-PGMA was tested with hDF. Glass discs coated with c-PGMA were put in contact with cell suspensions for 24 h after which the metabolically active cells were revealed using the MTT assay. Cell viability of hDF in contact with c-PGMA was not significantly different from hDF control cultures and hDF in contact with bare glass substrates, thereby proving the absence of cytotoxicity of c-PGMA. The results are shown in Fig. S4 (SM). PGMAs and their derivatives have been extensively proved to poses excellent in vivo and *in vitro* biocompatibility (Gupta et al., 2018; Li et al., 2014; Buzoglu et al., 2014; Wei et al., 2013; Yuan et al., 2012; Xiao et al., 2013; Bach et al., 2013).

Fig. 6A shows the cumulative release profile from Lys-loaded cPGMA in PBS at pH 7.4 for 14 days. The release of > 90% of charged Lys took place during the first 6 h, with all Lys passing to the PBS solution during the first 48 h. Fig. 6B shows the topographical analysis of the c-PGMA surface after the total removal of Lys. Fig. 6C represents the results of 5 consecutive recharges of Lys on the same cPGMA-functionalized substates, which were recharged for 24 h in a Lys solution with the same concentration. as stated below.

In all cases, the release of Lys was performed for 24 h in PBS pH 7.4 ensuring the total detachment of Lys from the surface. Fig. S5 (SM) shows FTIR spectra of Lys-loaded c-PGMA before and after Lys release that

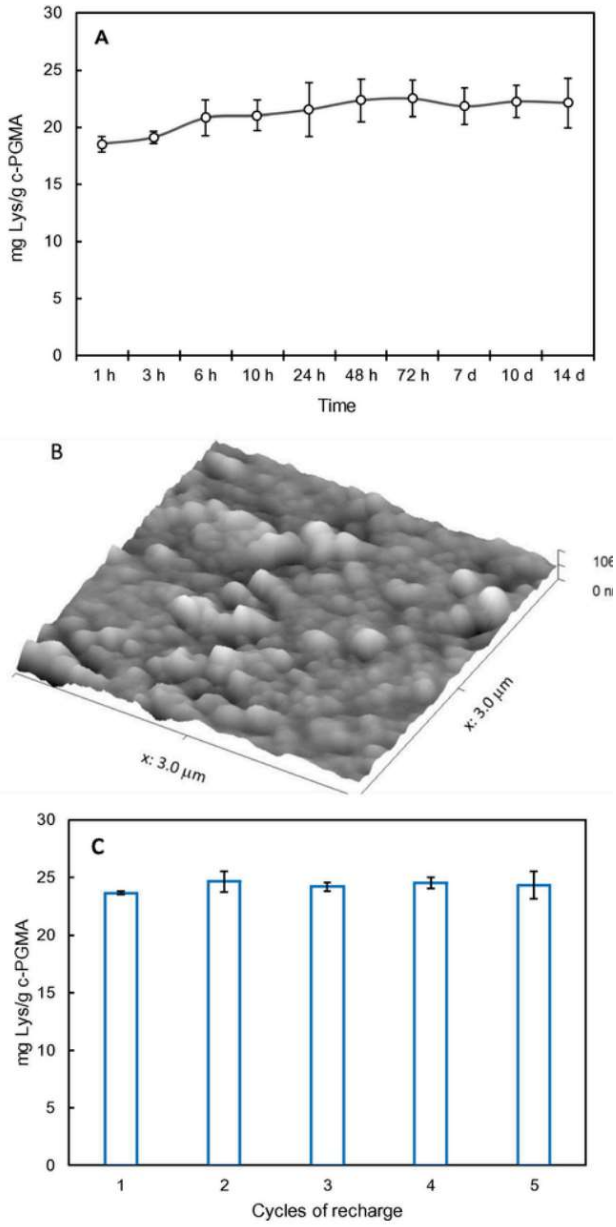

Figure 6. Cumulative release profile from Lys-loaded c-PGMA in PBS at pH 7.4 for 14 days (A), surface topography of c-PGMA surface after release of Lys by PBS solution (B) and results of the amount of Lys loaded after successive recharges on the same c-PGMA-functionalized surfaces (C).

closely matches the original c-PGMA spectrum. Few studies can be found for the use of PGMA-based materials with antimicrobial functionality incorporated. GMA-based polymers bearing cationic moieties were used for antimicrobial coated lenses showing high activity against methicillin-resistant *S. aureus* with good host cell viability (Pillai et al., 2020). The dispersion of silver NPs in amino functionalized PGMA also yielded a material with antibacterial activity (Deng et al., 2016). However, this is the first report of surface functionalization using cytocompatible GMA-polymers that makes use of its capacity to act as nanocarriers of antimicrobials.

4. Conclusions

In this work we prepared novel functional carrier platform for the AMP Lys from a flexible polymeric macromolecular assembly of crosslinked poly(glycidyl methacrylate) nanoparticles by typical selfassembly method. The incorporation of Lys to the c-PGMA yielded clear antimicrobial and anti-infective properties against the grampositive S. aureus and the gram-negative *E. coli.* even upon long administration period (14 days). The developed material displayed fast release within 24 h at physiological pH and complete reloading capacity without changes in the morphological characteristics of c-PGMA substates. In addition, c-PGMA material showed excellent biocompatibility to human dermal fibroblasts hDF. Overall, this study proves that macromolecular assemblies of crosslinked polymers can be used as biocompatible nanocarriers of AMPs with potential applications in biomedical field, such as drug/peptide delivery systems, wound dressings, bioactive scaffolds or anti-infective polymeric coatings for biomedical devices.

Acknowledgements

The authors acknowledge the funding provided by the Spanish Government (RTI2018-094840-B-C31) and the University of Alcala (CCG19/CC-037). LV thanks for FPU grant FPU17/03096 (Spanish Ministry of Education). GA thanks the University of Alcala for her postdoctoral fellowship. MP thanks the University of Alcala for his predoctoral fellowship. We thank ICTS "NANBIOSIS" for the Confocal Microscopy Service and TEM-Biophym Service (V. Souza-Egipsy) at the IEM-CSIC for the use of the facilities.

References

Abdelghany, S.M., Quinn, D.J., Ingram, R.J., Gilmore, B.F., Donnelly, R.F., Taggart, C. C., Scott, C. J., 2012. Gentamicin-loaded nanoparticles show improved antimicrobial effects towards *Pseudomonas aeruginosa* infection. Int. J. Nanomed. 7, 4053–4063.

Amariei, G., Kokol, V., Boltes, K., Letón, P., Rosal, R., 2018. Incorporation of antimicrobial peptides on electrospun nanofibres for biomedical applications. RSC Adv. 8, 28013–28023.

Bach, L.G., Islam, M.R., Lee, D.C., Lim, K.T., 2013. Poly(glycidyl methacrylate) grafted CdSe quantum dots by surface-initiated atom transfer radical polymerization: Novel synthesis, characterization, properties, and cytotoxicity studies. Appl. Surf. Sci. 283, 546–553.

Beaussart, A., Retourney, C., Quilès, F., Dos Santos-Morais, R., Gaiani, C., Fiérobe, H.P., El-Kirat-Chatel, S., 2021. Supported lysozyme for improved antimicrobial surface protection. J. Colloid Interface Sci. 582, 764–772.

Bridelli, M.G., 2017. Fourier transform infrared spectroscopy in the study of hydrated biological macromolecules. In: Fourier Transforms - High-tech Application and Current Trends. InTech Rijeka, pp. 191–213.

Buijs, J., Hlady, V.V., 1997. Adsorption kinetics, conformation, and mobility of the growth hormone and lysozyme on solid surfaces, studied with TIRF. J. Colloid Interface Sci. 190, 171–181.

Buzoglu, L., Maltas, E., Ersoz, M., Yildiz, S., 2014. Synthesis and characterization of PS-b-PGMA diblock copolymer and its interaction with blood proteins and donepezil. React. Funct. Polym. 82, 25–32.

Cassini, A., Högberg, L.D., Plachouras, D., Quattrocchi, A., Hoxha, A., Simonsen, G.S., Colomb-Cotinat, M., Kretzschmar, M.E., Devleesschauwer, B., Cecchini, M., Ouakrim, D.A., Oliveira, T.C., Struelens, M.J., Suetens, C., Monnet, D.L, the Burden of AMR Collaborative Group, 2019. Attributable deaths and disability-adjusted life-years caused by infections with antibiotic-resistant bacteria in the EU and the European Economic Area in 2015: a population-level modelling analysis. Lancet Infect. Dis. 19, 56–66.

Chen, X., Niyonsaba, F., Ushio, H., Okuda, D., Nagaoka, I., Ikeda, S., Okumura, K., Ogawa, H., 2005. Synergistic effect of antibacterial agents huma n β-defensins, cathelicidin LL-37 and lysozyme against *Staphylococcus aureus* and *Escherichia coli*. J. Dermatol. Sci. 40, 123–132.

Courdouan Tech. Application Note –Lysozyme-(cordouan-tech.com).

de la Fuente-Núñez, C., Reffuveille, F., Fernández, L., Hancock, R.E.W., 2013. Bacterial biofilm development as a multicellular adaptation: antibiotic resistance and new therapeutic strategies. Curr. Opin. Microbiol. 16, 580–589.

de Mélo-Silva, I.S., do Amorim, L.M., Rocha, A.M.O., da Costa, L.P., Tada, D.B., Franceschi, E., Padilha, F.F., 2020. Encapsulation of red propolis in polymer nanoparticles for the destruction of pathogenic biofilms. AAPS PharmSciTech 21, 49.

Deng, Y., Li, J., Pu, Y., Chen, Y., Zhao, J., Tang, J., 2016. Ultra-fine silver nanoparticles dispersed in mono-dispersed amino functionalized poly(glycidyl methacrylate) based microspheres as an effective anti-bacterial agent. React. Funct. Polym. 103, 92–98.

Deng, Y., Zhang, X., Shen, H., He, Q., Wu, Z., Liao, W., Yuan, M., 2020. Application of the nano-drug delivery system in treatment of cardiovascular diseases. Front. Bioeng. Biotechnol. 7.

Duan, Y., Liu, Y., Shen, W., Zhong, W., 2017. Fluorescamine labeling for assessment of protein conformational change and binding affinity in protein nanoparticle interaction. Anal. Chem. 89, 12160–12167.

Dutta, P., Ray, N., Roy, S., Dasgupta, A.K., Bouloussa, O., Sarkar, A., 2011. Covalent immobilization of active lysozyme on Si/glass surface using alkoxy Fischer carbene complex on SAM. Org. Biomol. Chem. 9, 5123–5128.

Duval, R.E., Grare, M., Demoré, B., 2019. Fight against antimicrobial resistance: We always need new antibacterials but for right bacteria. Molecules 24, 3152.

Flemming, H.C., Wingender, J., 2010. The biofilm matrix. Nat. Rev. Microbiol. 8, 623–633.

Green, R.J., Su, T.J., Lu, J.R., Penfold, J., 2001. The interaction between SDS and lysozyme at the hydrophilic solid-water interface. J. Phys. Chem. B 105, 1594–1602.

Gumustas, M., Sengel-Turk, C.T., Gumustas, A., Ozkan, S.A., Uslu, B., 2017. Effect of polymer-based nanoparticles on the assay of antimicrobial drug delivery systems. In: Grumezescu, A.M. (Ed.), Multifunctional Systems for Combined Delivery, Biosensing and Diagnostics. Elsevier, pp. 67–108.

Gupta, A., Landis, R.F., Li, C.H., Schnurr, M., Das, R., Lee, Y. -W., Yazdani, M., Liu, Y., Kozlova, A., Rotello, V.M., 2018. Engineered polymer nanoparticles with unprecedented antimicrobial efficacy and therapeutic indices against multidrug-resistant bacteria and biofilms. J. Am. Chem. Soc. 140, 12137–12143.

Henry, N., Clouet, J., Le Visage, C., Weiss, P., Gautron, E., Renard, D., Cordonnier, T., Boury, F., Humbert, B., Terr isse, H., Guicheux, J., Le Bideau, J., 2017. Silica nanofibers as a new drug delivery system: study of the protein silica interactions. J. Matter. Chem. B 5, 2908–2920.

Ivanova, E.P., Wright, J.P., Pham, D.K., Brack, N., Pigram, P., Alekseeva, Y. V., Demyashev, G.M., Nicolau, D.V., 2006. A comparative study between the adsorption and covalent binding of huma n immunoglobulin and lysozyme on surface-modified poly(tert-butyl methacrylate). Biomed. Ma ter. 1, 24–32.

Kaisersberger-Vincek, M., Strancar, J., Kokol, V., 2016. Antibacterial activity of chemically versus enzymatic functionalized wool with ε-poly-L-lysine. Text. Res. J. 87, 1604–1619.

Kim, J., Somorjai, G.A., 2003. Molecular packing of lysozyme, fibrinogen, and bovine serum albumin on hydrophilic and hydrophobic surfaces studied by infrared-visible sum frequency generation and fluorescence microscopy. J. Am. Chem. Soc. 125, 3150–3158.

Le, C.F., Fang, C.M., Sekaran, S.D., 2017. Intracellular targeting mechanisms by antimicrobial peptides. Antimicrob. Agents Chemother. 61.

Lee, D.H., Koh, E.H., Choi, S.R., Kim, S., 2013. Growth dynamics of *Staphylococcus aureus*, *Escherichia coli*, and *Pseudo monas aeruginosa* as a function of time to detection in BacT/alert 3D blood

culture bottles with various preincubation conditions. Ann. Lab. Med. 33, 406–409.
Li, Q.L., Gu, W.X., Gao, H., Yang, Y.W., 2014. Self-assembly and applications of poly(glycidyl methacrylate)s and their derivatives. Chem. Comm. 50, 13201–13215.
Liu, X., Ma, L., Chen, F., Liu, J., Yang, H., Lu, Z., 2019. Synergistic antibacterial mechanism of Bi2Te3 nanoparticles combined with the ineffective β-lactam antibiotic cefotaxime against methicillin-resistant *Staphylococcus aureus*. J. Inorg. Biochem. 196, 110687.
Lochmann, L., Pospíšil, J., Lím, D., 1966. On the interaction of organolithium compounds with sodium and potassium alkoxides. A new method for the synthesis of organosodium and organopotassium compounds. Tetrahedron Lett. 7, 257–262.
Mitchell, M.J., Billingsley, M.M., Haley, R.M., Wechsler, M.E., Peppas, N.A., Langer, R., 2020. Engineering precision nanoparticles for drug delivery. Nat. Rev. Drug Discovery. 20, 101–124.
Mosqueira, V.C.F., Loiseau, P.M., Bories, C., Legrand, P., Devissaguet, J.P., Barratt, G., 2004. Efficacy and pharmacokinetics of intravenous nanocapsule formulations of halofantrine in *Plasmodium berghei* infected mice. Antimicrob. Agents Chemother. 48, 1222.
Muñoz, M.T., Palenzuela, M., Cuenca, T., Mosquera, M.E.G., 2018. Aluminum aryloxide compounds as very active catalysts for glycidyl methacrylate selective ring-opening polymerization. ChemCatChem 10, 936–939.
Nečas, D., Klapetek, P., 2012. Gwyddion: an open-source software for SPM data analysis. Central Eur. J. Phys. 10, 181–188.
Ogunsona, E.O., Muthuraj, R., Ojogbo, E., Valerio, O., Mekonnen, T.H., 2020. Engineered nanomaterials for antimicrobial applications: A review. Appl. Mater. Today 18, 100473.
Palenzuela, M., Muñoz, M.T., Vega, J.F., Gutiérrez-Rodríguez, Á., Cuenca, T., Mosquera, M.E.G., 2019. Heterobimetallic aluminate derivatives with bulky phenoxide ligands: a catalyst for selective vinyl polymerization. Dalton Trans. 48, 6435–6444.
Pillai, S.K.R., Reghu, S., Vikhe, Y., Zheng, H., Koh, C.H., Chan-Park, M.B., 2020. Novel antimicrobial coating on silicone contact lens using glycidyl methacrylate and polyethyleneimine based polymers. Macromol. Rapid. Commun. 41, 2000175.
Ragland, S.A., Criss, A.K., 2017. From bacterial killing to immune modulation: Recent insights into the functions of lysozyme. PLOS Pathogens 13, e1006512.
Schmidt, C. F., Zimmermann, R.M., Gaub, H.E., 1990. Multilayer adsorption of lysozyme on a hydrophobic substrate. Biophys. J. 57, 577–588.
Searles, K., Tran, B.L., Pink, M., Chen, C.H., Mindiola, D.J., 2013. 3d early transition metal complexes supported by a new sterically demanding aryloxide ligand. Inorg. Chem. 52, 11126–11135.
Silhavy, T.J., Kahne, D., Walker, S., 2010. The bacterial cell envelope. Cold Spring Harbor Perspect. Biol. 2, a000414.
Sur, S., Rathore, A., Dave, V., Reddy, K.R., Chouhan, R.S., Sa dhu, V., 2019.
Recent developments in functionalized polymer nanoparticles for efficient drug delivery system. Nano-Struct. Nano-Objects 20, 100397.
Vahdati, M., Tohidi Moghadam, T., 2020. Synthesis and characterization of selenium nanoparticles-lysozyme nanohybrid system with synergistic antibacterial properties. Sci. Rep. 10, 510.
Vázquez-Muñoz, R., Meza-Villezcas, A., Fournier, P.G.J., Soria-Ca stro, E., Juarez-Moreno, K., Gallego-Hernández, A.L., Bogdanchikova, N., Vazquez-Duhalt, R., Huerta-Saquero, A., 2019. Enhancement of antibiotics antimicrobial activity due to the silver nanoparticles impact on the cell membrane. PLoS One 14, e0224904.
Wang, L., Hu, C., Shao, L., 2017. The antimicrobial activity of nanoparticles: present situation and prospects for the future. Int. J. Nanomed. 12, 1227–1249.
Wang, N., Cheng, X., Li, N., Wang, H., Chen, H., 2019. Nanocarriers and their loading strategies. Adv. Healthcare Ma ter. 8, 1801002.
Wei, H., Pahang, J.A., Pun, S.H., 2013. Optimization of brush-like cationic copolymers for nonviral gene delivery. Biomacromolecules 14, 275–284.
Wertz, C. F., Santore, M.M., 2002. Adsorption and reorientation kinetics of lysozyme on hydrophobic surfaces. Langmuir 18, 1190–1199.
Wilczewska, A.Z., Niemirowicz, K., Markiewicz, K.H., Car, H., 2012. Nanoparticles as drug delivery systems. Pharmacol. Rep. 64, 1020–1037.
Xiao, L., Tong, Z., Chen, Y., Pochan, D.J., Sabanayagam, C. R., Jia, X., 2013. Hyaluronic acid-based hydrogels containing covalently integrated drug depots: Implication for controlling inflammation in mechanically stressed tissues. Biomacromolecules 14, 3808–3819.
Ye, Y., Klimchuk, S., Shang, M., Niu, J., 2019. Improved antibacterial performance using hydrogel-immobilized lysozyme as a catalyst in water. RSC Adv. 9, 20169–20173.
Yuan, S., Xiong, G., Roguin, A., Choong, C., 2012. Immobilization of gelatin onto poly (glycidyl methacrylate)-grafted polycaprolactone substrates for improved cell–material interactions. Biointerphases 7, 30.
Zhang, B., Tao, H., Niu, X., Li, S., Chen, H.Q., 2017. Lysozyme distribution, structural identification, and in vitro releas e of starch-based microgel lysozyme complexes. Food Chem. 227, 137–141.
Zhang, L.J., Gallo, R.L., 2016. Antimicrobial peptides. Curr. Biol. 26, R14–R19.

Supplementary Material

Poly(glycidyl methacrylate) macromolecular assemblies as biocompatible nanocarrier for the antimicrobial lysozyme

Miguel Palenzuela[1], Laura Valenzuela[2], Georgiana Amariei[2,*], Juan F. Vega[3], Marta E.G. Mosquera[1,*], Roberto Rosal[2]

[1] Department of Organic and Inorganic Chemistry, Institute of Chemical Research "Andrés M. del Río" (IQAR), Universidad de Alcalá, 28805 Alcalá de Henares, Madrid, Spain
[2] Department of Chemical Engineering, Universidad de Alcalá, 28805 Alcalá de Henares, Madrid, Spain.
[3] Department of Macromolecular Physics, Instituto de Estructura de la Materia, IEM-CSIC, 28006 Madrid, Spain

Contents

Int. J. Pharm. 603, 120695, 2021

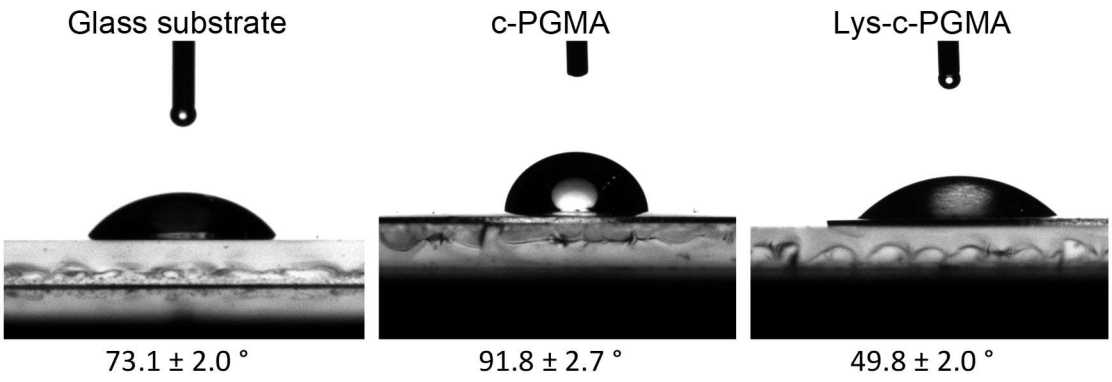

Figure S1. Water contact angle (°) on glass substrate (left), c-PGMA deposited on glass substrate (centre) and Lys-loaded c-PGMA (right).

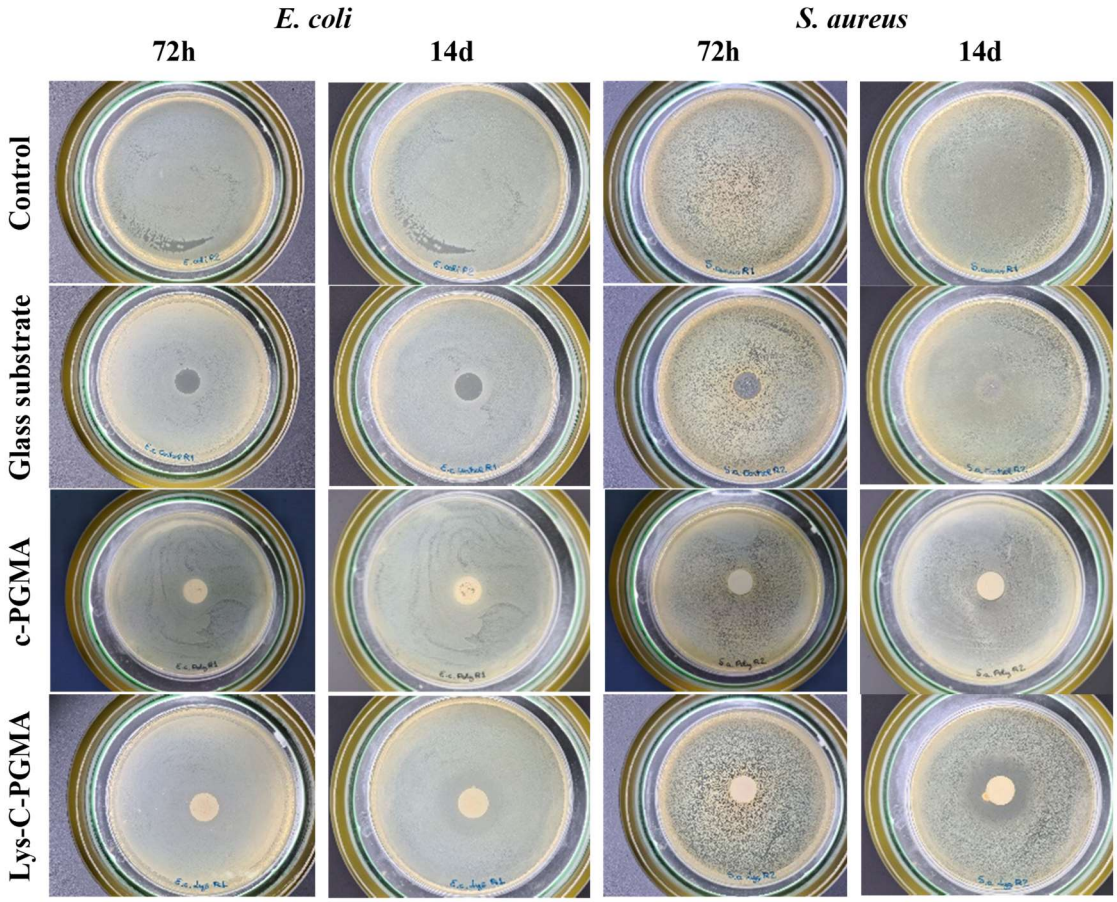

Figure S2. Representative images of *inhibition* zone experiments corresponding to glass substrate, c-PGMA deposited on glass substrate, Lys-loaded c-PGMA, and negative control along 14-day in contact with *E. coli* and *S. aureus*, at 37°C. Zones of bacterial growth inhibition are marked by clear zones.

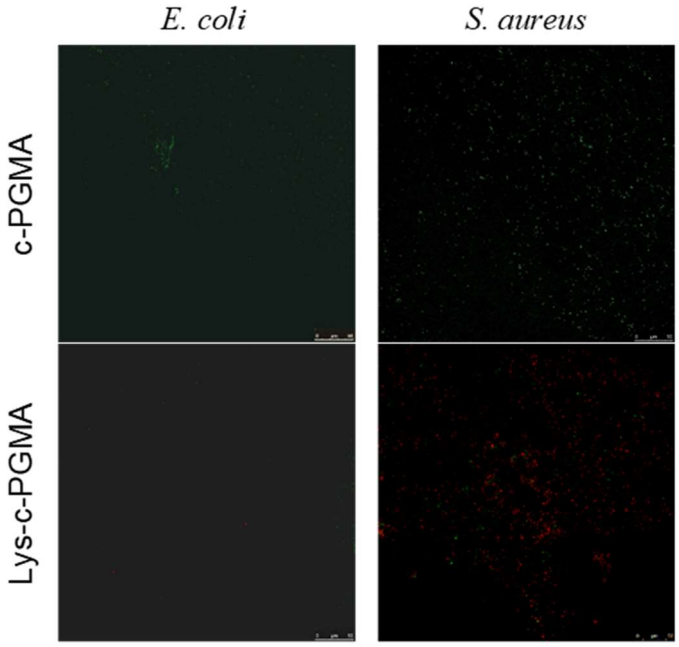

Figure S3. Confocal Live/Dead micrographs (scale bar 50µm) of specimens of glass substrates covered with c-PGMA and Lys-c-PGMA in contact with *E. coli* and *S. aureus* cultures after 20 h.

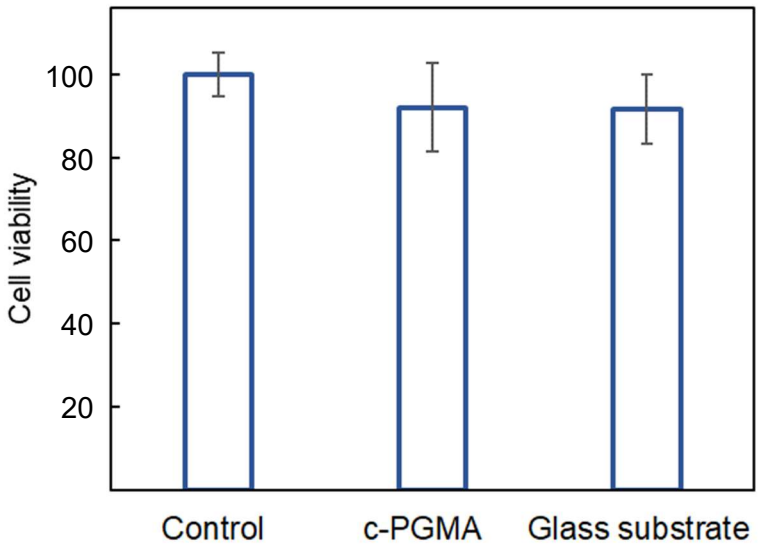

Figure S4. Results of the MTT assay for the biocompatibility of c-PGMA with human dermal fibroblasts. (Cell viability expressed with respect to control = 100.)

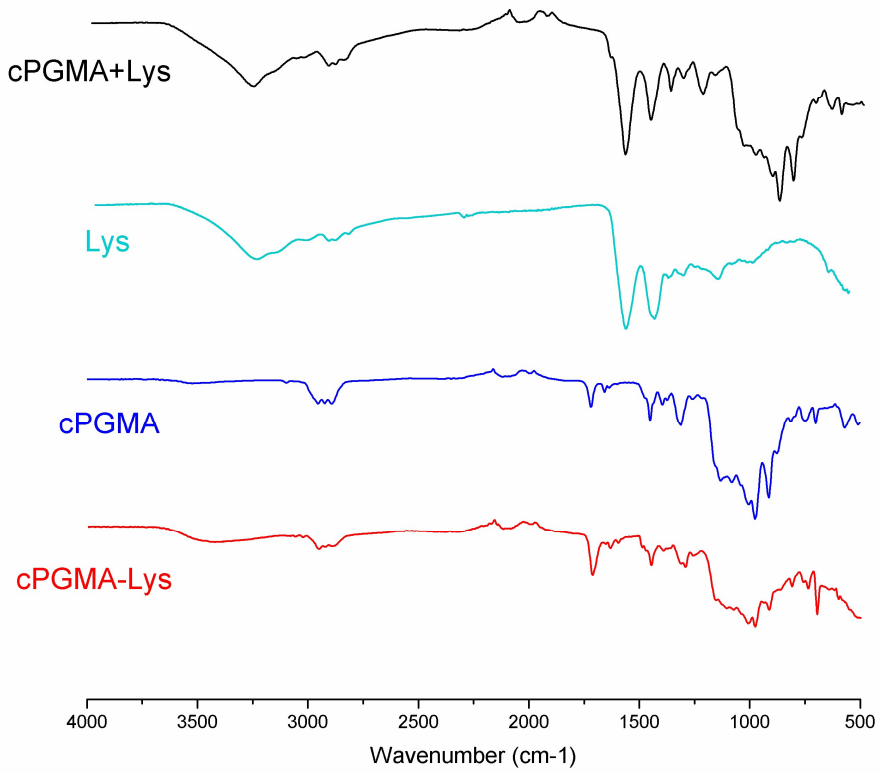

Figure S5. FTIR comparative spectra of Lys-loaded c-PGMA (cPGMA+Lys) (black) free Lys (turquoise), free cPGMA (blue) and Lys-unloaded c-PGMA (cPGMA-Lys) (red).